

# A Fracture-Mechanics-Based Approach to Fracture Control in Biomedical Devices Manufactured From Superelastic Nitinol Tube

S. W. Robertson, R. O. Ritchie

Department of Materials Science and Engineering, University of California, Berkeley, California 94720

Received 8 September 2006; revised 31 January 2007; accepted 6 March 2007

Published online 5 May 2007 in Wiley InterScience (www.interscience.wiley.com). DOI: 10.1002/jbm.b.30840

**Abstract:** Several key fracture-mechanics parameters associated with the onset of subcritical and critical cracking, specifically the fracture toughness, crack-resistance curve, and fatigue threshold, have recently been reported for the superelastic alloy Nitinol, in the product form of the thin-walled tube that is used to manufacture several biomedical devices, most notably endovascular stents. In this study, we use these critical parameters to construct simple decision criteria for assessing the quantitative effect of crack-like defects in such Nitinol devices with respect to their resistance to failure by deformation or fracture. The criteria are based on the (equivalent) crack-initiation fracture toughness and fatigue threshold stress-intensity range, together with the general yield strength and fatigue endurance strength, and are used to construct a basis for design against single-event (overload) failures as well as for time-/cycle-delayed failures associated with fatigue. © 2007 Wiley Periodicals, Inc. *J Biomed Mater Res Part B: Appl Biomater* 84B: 26–33, 2008

**Keywords:** Nitinol; fracture mechanics; fatigue; fracture toughness

## INTRODUCTION

Nitinol, a nearly equiatomic alloy of Ni and Ti, is widely used by the biomedical community for implant devices in part because of its unique characteristics of superelasticity, *in vivo* corrosion resistance, and radioopacity. The alloy is particularly suited for self-expanding stents; indeed, Nitinol endovascular stents constitute nearly 60% of a rapidly expanding market.<sup>1</sup> However, there have been several reports of *in vivo* fractures of devices made from Nitinol, some resulting in little harm to the patient, but others coincident with complete device failure and serious health complications.<sup>2–4</sup> Despite this, studies are relatively rare on the fracture and fatigue-crack growth properties of thin-walled superelastic Nitinol tube, the raw product form that is used to manufacture many of these devices.

To address this deficiency, recent work has focused on characterizing fracture and crack growth in such Nitinol thin-walled tubing, which is the primary product form used in the manufacture of Nitinol stents. These materials have tensile transformation stresses of  $\sim 400$  MPa (at  $\sim 1\%$  strain) and a (martensite) yield stress of  $\sigma_y \sim 1000$  MPa.

Specifically, the fracture toughness behavior, in the form of crack-resistance curves (R-curves), and the fatigue-crack growth properties, including the fatigue-crack growth threshold stress-intensity range, have been measured in air and a simulated body fluid of 37°C Hanks' Balanced Saline Solution (HBSS).<sup>5,6</sup> Through the use of these parameters, we present simple conservative criteria for assessing the quantitative effect of crack-like defects in such Nitinol devices with respect to their resistance to fracture.

## PROCEDURES

As noted earlier, the relevant fracture mechanics data used in this work are taken from Refs. 5 and 6 for  $\sim 400$ - $\mu\text{m}$ -thick thin-walled superelastic Nitinol tubing (composition, Ti – 50.8 at % Ni), similar to that used for manufacture of self-expanding stents. Measurements were made on 370–410- $\mu\text{m}$ -thick compact-tension C(T) specimens, laser-machined (and then electropolished) from unrolled and shape-set flattened tube and heat treated to mimic commercial shape-setting procedures utilized in stent manufacture; this resulted in material with an austenite finish temperature of  $A_f \sim 25$ – $30^\circ\text{C}$ , i.e., which is superelastic at body temperatures.

Data on fatigue-crack growth rates [Figure 1(a,b)] were obtained from measurements made in 37°C HBSS (pH of 7.4) on C(T) samples with a prenotch oriented 45° to the tube drawing axis (energetically the most favorable fatigue crack path<sup>5,6</sup>); tests involved cycling at 50 Hz (sine wave)

Correspondence to: R. O. Ritchie (e-mail: RORitchie@lbl.gov)

Contract grant sponsor: National Science Foundation; Contract grant number: CMS-0409294

Contract grant sponsor: Nitinol Devices and Components, Inc., a Johnson and Johnson Company, Fremont, CA

© 2007 Wiley Periodicals, Inc.

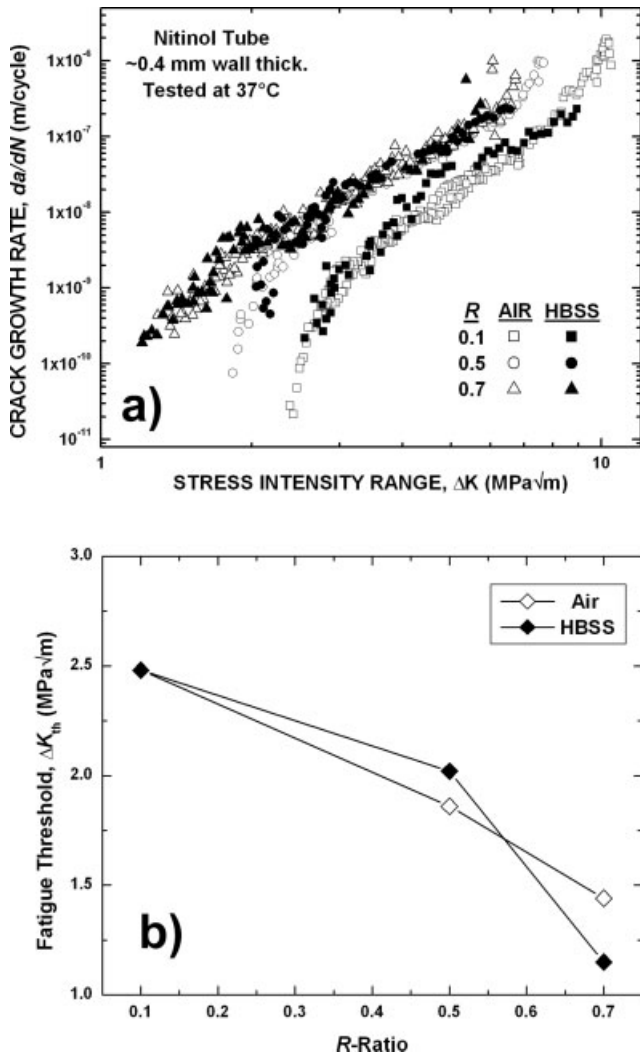


**Figure 1.** Fatigue data from thin-walled superelastic Nitinol tube tested in 37°C air<sup>5</sup> and Hanks' Balanced Saline Solution (HBSS)<sup>6</sup> showing (a) fatigue-crack growth rates as a function of stress-intensity range  $\Delta K$ , and (b) the variation in fatigue threshold values with the load ratio ( $K_{min}/K_{max}$ ).

at positive load ratios ( $R =$  ratio of minimum to maximum load) between 0.1 and 0.7, with the fatigue threshold,  $\Delta K_{th}$ , operationally defined, as per ASTM E 647,<sup>7</sup> as the stress-intensity range,  $\Delta K = K_{max} - K_{min}$ ,\* to give a growth rate,  $da/dN$ , of  $10^{-10}$  m/cycle (based on linear extrapolation of data between  $10^{-9}$  and  $10^{-10}$  m/cycle) [Figure 1(b)].<sup>†</sup>

Fracture toughness data reflect crack-resistance (R-curve) measurements<sup>8</sup> made in 37°C air on fatigue pre-

\* The stress-intensity factor,  $K$ , is a global parameter which fully characterizes the local stress and deformation fields in the immediate vicinity of a crack tip, and thus can be used to correlate to the extent of crack advance. In its most basic form, the stress-intensity factor is defined for a crack of length (or half length)  $a$  as  $K = Y\sigma_{app}(\pi a)^{1/2}$ , where  $\sigma_{app}$  is the applied stress and  $Y$  is a geometry factor of order unity. Handbook solutions are available for the geometry factor,  $Y$ , as well as more complex formulations of  $K$  for specific geometries.<sup>7,8</sup> Intricate geometries such as stents may require the use of finite-element simulations to numerically calculate specific  $K$  solutions, and to relate stresses to strains.

† For such a stress-intensity-based characterization of crack advance, small-scale yielding conditions are generally needed to prevail. This necessitates that the extent of local plasticity at the crack tip, that is, the plastic-zone size [ $r_y \sim 1/2\pi(K/\sigma_y)^2$ ], should be some 10 times or more smaller than the in-plane dimensions of crack length and remaining uncracked ligament size.<sup>7,8</sup>

cracked C(T) specimens with prenotches oriented longitudinal (parallel), at 45°, or circumferential to the drawing direction [Figure 2].<sup>6</sup> As cracking in some instances was inclined at an angle to the mode I ( $K_{II} = 0$ ) crack path, fracture toughness values are given as equivalent toughness,  $K_{eq}$ , values, computed from the strain-energy release rate in terms of both on mode I and mode II components.<sup>6</sup>

**RESULTS**

**Time/Cycle Delayed Failure (Fatigue)**

Many biomedical devices manufactured from Nitinol tube are subjected to relatively constant and repetitive stress amplitudes. For example, stents implanted in arteries are exposed to contractions and dilations at roughly 1.2 Hz due to the human heartbeat; typically, this results in 3–10% diameter changes in the luminal wall with a pulse pressure of ~100 mmHg.<sup>9</sup> Peripheral stents may be subjected to additional cyclic stresses due to musculoskeletal motions, e.g., knee flexion during walking. Such cyclic deformation can lead to the generation of accumulated fatigue damage in the device, which may eventually result in the propagation of fatigue cracks. Typical data of the variation in fatigue-crack growth rates with the stress-intensity range,  $\Delta K$ , in thin-walled superelastic Nitinol tube is shown in Figure 1. A critical parameter in this plot for biomedical device design is the threshold value,  $\Delta K_{th}$ , below which crack growth is presumed to be dormant. Because of their small-section geometry, combinations of applied stresses and crack sizes leading to stress intensities much above the

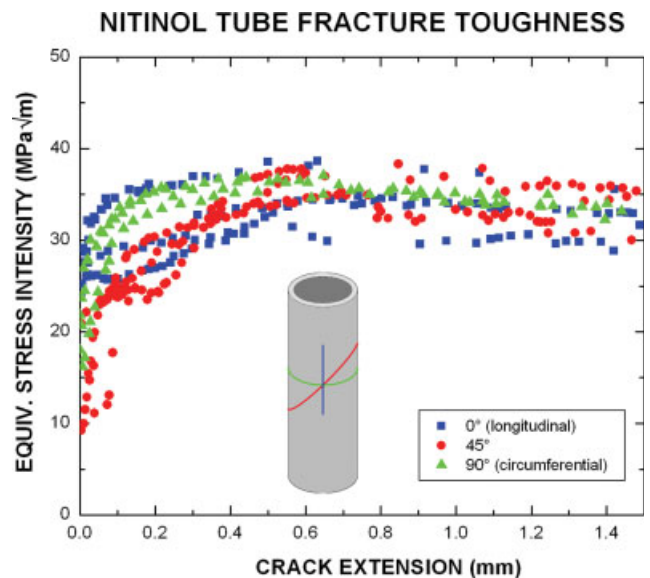


**Figure 2.** Fracture toughness in terms of crack-resistance (R-curve) data for thin-walled superelastic Nitinol tube tested in 37°C air. Crack-initiation toughness values were significantly lower than those at steady-state, and depended strongly on crack-propagation direction within the tube (after Ref. 6). [Color figure can be viewed in the online issue, which is available at [www.interscience.wiley.com](http://www.interscience.wiley.com).]

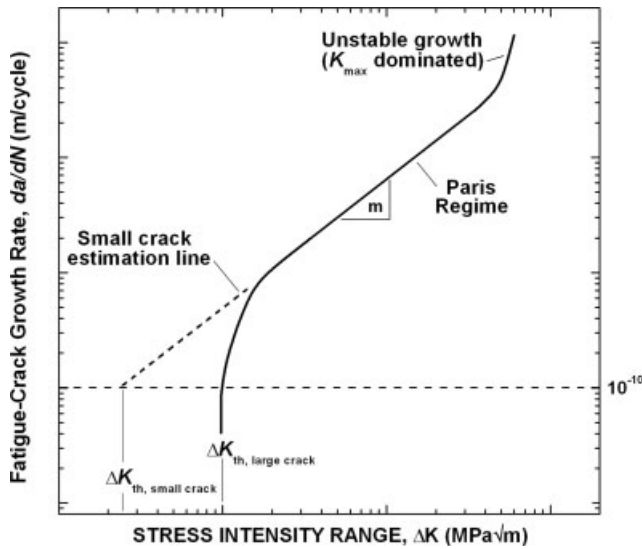


**Figure 3.** A typical fatigue-crack growth-rate curve plotted in log-log scale with critical locations marked. Threshold values,  $\Delta K_{th}$ , for large cracks are determined from experimental data collected using standard fracture-mechanics specimens and typically represent the asymptotic stress-intensity range for crack growth. This asymptote of the data in Nitinol tube is invariably due to crack closure effects from interference or wedging of oxidation debris or fracture surface asperities inside the crack flanks. Physically small cracks, however, are more relevant to commercial biomedical devices, and are not subjected to the same closure effects as are laboratory-grown large cracks; consequently, they may propagate at stress intensities lower than predicted by large-crack data. Estimates of the threshold stress-intensity range for small cracks can be made by extrapolation of the linear Paris growth-rate curve down to  $10^{-10}$  m/cycle. For small-scale biomedical devices such as endovascular stents that are only a few hundred micrometers thick in specific regions, any stress-intensity ranges above the  $\Delta K_{th}$  value, that is, in the Paris or unstable growth regime, can result in rapid through-thickness fracture. Accordingly, the threshold  $\Delta K_{th}$  value can be considered as the critical limiting variable.

threshold value can lead to the growth of such cracks and premature failure of the device. Consequently, for safe *in vivo* operation, it is desirable that stress-intensity conditions remain below the threshold.

Conventionally, the fatigue threshold is operationally defined as the stress-intensity range to yield a growth rate less than  $10^{-10}$  m/cycle.<sup>7</sup> However, this rather arbitrary assignment of the threshold, which for physiological frequencies translates to crack extensions of  $\sim 4$  mm per year, is somewhat precarious when dealing with small devices such as stents which may contain physically small flaws. Unlike the relatively large cracks, typically millimeters in length, found in laboratory fatigue specimens, biomedical devices are likely to contain far smaller flaws on the order of tens of micrometers in size, for example, microstructural voids, inclusions, or crack-like defects.<sup>10</sup> Thresholds for such small cracks tend to be lower than the large-crack thresholds (this is sometimes referred to as the “small-crack effect”<sup>11</sup>). Although difficult to measure precisely by experiment, such small-crack thresholds can be usefully estimated by extrapolating the linear, mid growth-rate, portion of the  $da/dN$  vs.  $\Delta K$

**TABLE I.** Fatigue-Crack Growth  $\Delta K_{th}$  Thresholds for Thin-Walled Superelastic Nitinol Tube as a Function of Load Ratio,  $R$

$R$	$\Delta K_{th}$ (MPa $\sqrt{m}$ )	
	Large Crack	Small Crack
0.1	2.48	1.33
0.5	2.02	0.81
0.7	1.15	0.71

Threshold values are shown for both large cracks from experimental results and for small cracks based on a linear extrapolation of the Paris regime.<sup>6</sup>

curve, i.e., the Paris regime,<sup>‡</sup> to lower growth rates<sup>12</sup> (as shown schematically in Figure 3). Mechanistically, this can be justified by noting that due to their limiting wake, small cracks do not develop significant levels of crack closure, that is, microscopic crack wedging processes primarily due to oxide debris or asperity contact inside the crack, which act to effectively lower the near-tip  $\Delta K$  by increasing  $K_{min}$ <sup>14–16</sup>; such closure tends to prematurely “arrest” cracks, leading to asymptotic crack-growth behavior at the large-crack threshold.

Fatigue-crack growth rates and corresponding threshold values in Nitinol thin-walled tube (Figure 1) are sensitive to load ratio but relatively insensitive to test frequency.<sup>6</sup> Measured large-crack threshold values are listed in Table I<sup>6</sup>; note that higher  $R$  values lead to lower  $\Delta K_{th}$  values [Figure 1(b)]. Small-crack fatigue thresholds are estimated from the Paris-law constants  $C$  and  $m$ , according to the equation

$$\Delta K_{th, \text{small crack}} = \left( \frac{10^{-10}}{C} \right)^{1/m} \quad (1)$$

Extrapolation of the  $R = 0.5$  data at 1 Hz<sup>6</sup> resulted in  $\sim 9\%$  lower small-crack threshold values when compared with the same data from the higher (unrealistic) 50 Hz frequency test. Therefore, all small-crack  $\Delta K_{th}$  threshold values estimated from 50 Hz data are reduced by 9% in Table I to account for the difference between the experimental test frequency and *in vivo* conditions.

### Overload Failure (Toughness)

In addition to failures that can occur after a period of time in use, biomedical devices are sometimes subjected to conditions that can cause single-event overloads leading to instantaneous failures. In stents, these events include crimping to fit inside a catheter, tortuous maneuvering into the appropriate anatomic position, and actual deployment. These single-event overloads require much more energy (by an order of magnitude or more) for fracture than the cumulative effects of fatigue damage, and for this reason

<sup>‡</sup> In the Paris regime, which typically occurs between growth rates of  $10^{-9}$  and  $10^{-6}$  m/cycle, growth rates can be simply expressed as a power-law function of stress intensity; in its simplest form, this gives rise to the so-called Paris power law<sup>13</sup>:  $da/dN = C\Delta K^m$ , where  $C$  and  $m$  are experimentally determined scaling constants.

**TABLE II. Equivalent Fracture Toughness Values for Thin-Walled Superelastic Nitinol Tube Computed From Maximum Strain-Energy Release Rates to Compensate for Angled Crack Growth in the Circumferential Direction**

Orientation	$K_{eq}$ (MPa√m)	
	Crack-Initiation	Steady-State
Longitudinal	27	36
45°	10	34
Circumferential	16	33

Toughness data show a rapid increase in fracture toughness from low crack-initiation values to a steady-state value of  $\sim 34$  MPa√m after  $\sim 400$   $\mu$ m of crack growth.<sup>6</sup>

have a much lower probability of occurring. However, it is pertinent to consider the possibility of such fractures in any comprehensive criteria for device failure.

Fracture toughness values reported for superelastic Nitinol tubing show dependence on both the extent of crack advance,

as characterized by the R-curve, and the orientation of the crack path within the tube (Table II). Specifically, toughness values for crack initiation are lowest ( $K_{eq} \sim 10$  MPa√m) for cracks growing at 45° to the axis of the tube, and highest ( $K_{eq} \sim 27$  MPa√m) for cracks growing longitudinally, with  $K_{eq} \sim 16$  MPa√m for the circumferential crack-growth orientation. Following such initiation, the toughness rises rapidly before reaching a steady-state value of  $K_{ss} \sim 34$  MPa√m, which is nominally the same for all orientations, after  $\sim 400$   $\mu$ m of crack extension<sup>6</sup> (Figure 2). Although the precise origin of such R-curve behavior is not fully understood—there is clearly a role of texture and competing effects ahead of the crack tip (intrinsic damage) and in the plastic/superelastic crack wake (extrinsic crack-tip shielding)—from the perspective of developing conservative design criteria for Nitinol devices, the lower-bound crack-initiation toughness is the parameter of relevance. When local stress intensities are below this value, the device can be considered to be safe from instantaneous overload fracture.

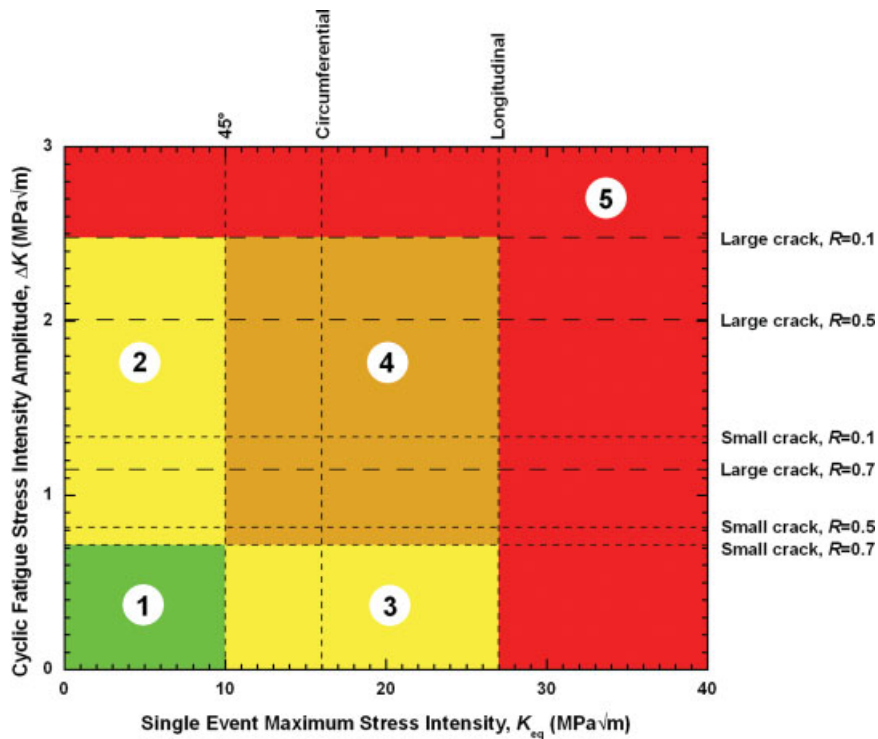


**Figure 4.** A fracture-mechanics-based safe-operating device design diagram is shown for devices manufactured from thin-walled superelastic Nitinol tube. Stress intensities attributed to single events, for example, crimping and deployment stresses in a stent, are represented on the horizontal axis and vary by the angle that the crack is propagating with respect to the tube-drawing direction. Stress-intensity ranges attributed to cyclic events, for example, contraction and dilation of a stent in response to the heartbeat or musculoskeletal motion, are represented on the vertical axis and vary with load ratio,  $R$ , and whether the experimental large-crack fatigue data or the more conservative small-crack estimates are used. Any combination of defect sizes and single-event stresses and/or cyclic stresses falling into region 1 pose no threat of fracture or crack propagation under the evaluated conditions. Devices whose stress intensities fall in regions 2 and 3 are mildly susceptible (depending on exact  $R$ -ratio and crack-growth directions) to fatigue-crack growth and fracture, respectively; in region 4, the device is susceptible to fracture by either mechanism. Parts that are subjected to any portion of region 5 are in great risk of fracture either by fatigue or by overload, regardless of the crack angle and  $R$ -ratio. [Color figure can be viewed in the online issue, which is available at [www.interscience.wiley.com](http://www.interscience.wiley.com).]

## DISCUSSION

### Stress Intensity Factor Based Device Design Diagram

Mechanical analysis to calculate the stresses experienced by a biomedical device, which is most easily performed by finite-element modeling, can reveal the maximum stress intensities generated at presumed worst-case defects during single-event type occurrences, such as deployment of the stent, and the stress-intensity range (and load ratio) attributed to cyclic deformation (see, for example, Ref. 17). In addition, such analyses can be used to reveal “critical locations” on the biomedical device where cracking problems may arise; these are usually defined as regions of particularly high stress/strain, or where experimental testing or *in vivo* data have shown that cracking events may occur.

By considering the computed stress-intensity values at such critical locations, and comparing them to the critical fracture mechanics parameters of the fracture toughness and fatigue threshold, regions of safe operation can be mapped out in terms of the applied stresses and likely defect sizes. Conservative values here would pertain to the crack-initiation fracture toughness for the appropriate (or worst-case 45°) orientation, and the threshold stress-intensity range for worst-case small cracks at an appropriate (or worst-case highest) load ratio. Figure 4 presents such a safe-operating device design diagram based on the fracture mechanics data for Nitinol thin-walled tubing described in this work; this diagram readily permits a quick assessment of the susceptibility of a particular device to failure by time/cycle delayed fatigue or to instantaneous fracture due to an overload. Specifically, the maximum stress intensity produced during single-event type occurrences is represented by the  $x$  position on the grid, and the stress-intensity range attributed to cyclic events is plotted as the  $y$  coordinate. The location of the  $(x,y)$  positional pair on the plot then reveals if the device is susceptible to fatigue-crack growth, overload fracture, or both. Using worst-case values, region 1 in Figure 4 represents the area that is safe from fatigue-crack growth and overload fracture under all conditions analyzed ( $R = 0.1$ – $0.7$ , crack-growth angle = longitudinal, 45°, and circumferential). Regions 2 and 3 represent a degree of susceptibility to fatigue-crack growth and overload fracture, respectively; region 4 represents the unsafe region where the device would be susceptible to both modes of failure. Depending on the individual device mechanics, for example, if the *in vivo* operating conditions are such that  $R < 0.7$ , and/or the crack path is nearer the circumferential or longitudinal direction, the safe zone (Region 1) may be expanded to encompass all, or parts of, regions 2–4. Region 5 represents the worst-case scenario where failure by overload fracture or fatigue-crack growth is an eminent risk.

### Stress and Flaw Size Based Device Design Diagram

An alternative, and perhaps more insightful, approach to safe design criteria, using applied stresses and flaw sizes (rather than stress-intensity factors as in Figure 4), is afforded by the Kita-

gawa-Takahashi diagram.<sup>18</sup> For modeling the threshold conditions for fatigue, this approach combines a fracture-mechanics-based “damage tolerant” approach, which defines a large-crack limit (in terms of the fatigue threshold  $\Delta K_{th}$ ), with the more traditional “total-life” ( $S/N$ ) approach, which is used to define a small-crack limit in terms of the fatigue limit (or endurance strength)  $\Delta\sigma_{fat}$ . The benefit of such a combination is that the traditional approach quantifies the effects of crack nucleation and propagation from small, often blunt, flaws that are present in as-manufactured parts, and relates this to the typical data collected from damage-tolerant ( $da/dN$  vs.  $\Delta K$ ) experiments. The  $10^6$ -cycle endurance strength,  $\Delta\sigma_{fat}$ , determined for tension–tension fatigue testing in Nitinol tube, varies with heat treatment and  $R$ -ratio, and ranges from 100 to 200 MPa.<sup>19,20</sup> For corresponding modeling of overload failure, the diagram combines the fracture toughness of the material as the large-crack limit and the general yield stress, that is, limit-load stress for plastic failure, at the small-crack limit. For this particular example, the general yield stress was estimated as simply the uniaxial (0.2% offset) yield stress, from the linear-elastic martensite loading curve,  $\sigma_y^{mart}$ , for Nitinol tubing; this ranges from 1000 to 1200 MPa.<sup>21,22§</sup>

Figure 5 shows the constructed Kitagawa-Takahashi diagram for thin-walled superelastic Nitinol tube. The intersection of the damage-tolerant fatigue curves and the endurance strength represents the transition from large to small crack fatigue behavior. In the case of Nitinol tubing, this transition (sometimes referred to as the intrinsic crack size) occurs at  $\sim 15$ – $50 \mu\text{m}$ . Devices with flaws below this length scale are best analyzed in terms of the endurance strength in fatigue and general yield strength in single-event overloads, whereas fracture mechanics provides the more appropriate means of analysis for flaws larger than this scale, specifically in terms of the fatigue threshold,  $\Delta K_{th}$ , and fracture toughness,  $K_{eq}$ . Since ASTM standards<sup>10</sup> for Nitinol biomedical devices allow inclusion and porosity sizes up to  $39 \mu\text{m}$ , which is within this transitional flaw size range, this clearly demonstrates the necessity of using both the traditional fatigue evaluation techniques and fracture-mechanics-based criteria in the assessment of the safety of any device. The steady-state fracture toughness,  $K_{ss}$ , is reached following  $\sim 400 \mu\text{m}$  of crack extension, which results in the horizontal transition lines from the longitudinal, circumferential, and 45° crack-initiation toughness-based curves to the steady-state curve at that value of crack size,  $a$ , although with such crack sizes, small-scale yielding conditions are no longer likely to apply.<sup>¶</sup> The importance of the Kitagawa-Takahashi diagram for Nitinol is

§ Note that for the purposes of constructing this generic Kitagawa-Takahashi diagram for superelastic Nitinol thin-walled tubing, we have plotted the fracture mechanics data, that is, the fatigue threshold and fracture toughness, in terms of the simple relationship  $\Delta\sigma = \Delta K_{th}/Y(\pi a)^{1/2}$  for fatigue conditions, and  $\sigma_{max} = K_{eq}/Y(\pi a)^{1/2}$  for overload conditions, with the geometry factor,  $Y$ , taken equal to unity. Similarly, we have considered the corresponding general yield stress in terms of simple uniaxial tensile loading. However, computation of the actual variation in these limiting stresses for fatigue and overload failure for specific applications will clearly vary with the crack configuration, the nature of the loading, and the particular device geometry.

¶ It should be noted that crack sizes larger than  $\sim 100 \mu\text{m}$  are highly unlikely in biomedical devices with dimensions measured in terms of fractions of millimeters; however, they have been included in the diagram for completeness.

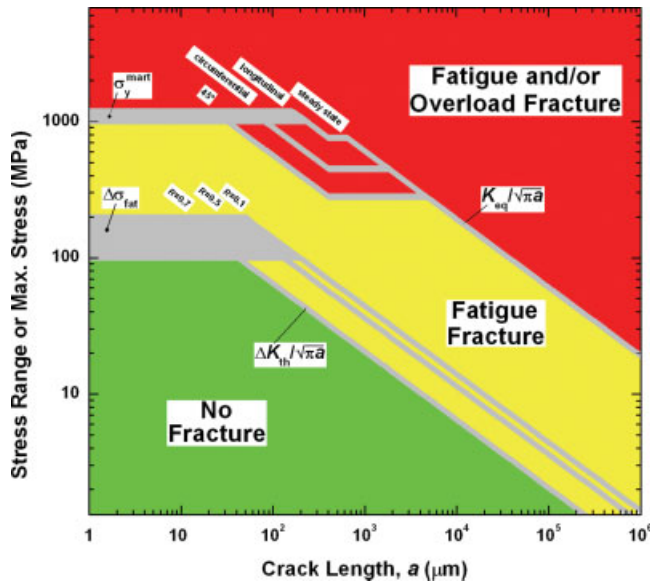


**Figure 5.** Kitagawa-Takahashi diagram for thin-walled superelastic Nitinol tubing showing regions of safe operation (green), risk of failure by fatigue but not overload fracture (yellow), and eminent risk of failure by either fatigue or by overload fracture. The transition crack-size between small-crack behavior, governed by the stress-life endurance strength (100–200 MPa<sup>19,20</sup>), and large-crack fracture mechanics data is ~15–50 μm. Above that flaw size, fatigue fracture is best defined by the fracture mechanics-based threshold criterion  $\Delta K_{th}$ , which is a function of the positive load-ratio,  $R$ . Failure by overload is bounded by the martensitic yield stress for Nitinol tube (1000–1200 MPa<sup>21,22</sup>) up to a flaw size of ~25 μm, at which point the crack-initiation fracture toughness of the material dominates failure. For crack sizes exceeding ~400 μm, the steady-state fracture toughness value (~34 MPa√m) governs the point of fracture, hence the jump from the longitudinal, circumferential, and 45° safe operating curves. It should be noted that for the purposes of determining this particular diagram, the geometry factor  $Y$  was taken as unity and general yield stress defined in uniaxial tension. For an actual device, these would have to be calculated for the specific loading, crack and device geometry. [Color figure can be viewed in the online issue, which is available at [www.interscience.wiley.com](http://www.interscience.wiley.com).]

that it provides an alternative design diagram, now presented in terms of applied stresses and flaw sizes, instead of stress intensities, to indicate regions of safe operation (green), risk of failure by time- or cycle-delayed fatigue but not overload failure (yellow), and eminent risk of failure by either fatigue or overload fracture/general yielding.

**Limitations of the Analysis**

In this analysis, we have used fracture mechanics and the specific parameters of the fatigue threshold and fracture toughness as a basis for defining the stresses and crack sizes for safe operation of any given device. However, it should be noted that such fracture mechanics approaches are in no way a substitute for traditional life-prediction methodologies based on stress- or strain-life fatigue. We believe that these two approaches to fatigue design are complimentary, and as shown in Figure 5 they can be com-

bined to give a more comprehensive description of behavior. In essence, traditional stress-/strain-life fatigue applies in the absence of cracks (or when they are too small to be considered), whereas fracture mechanics provides a means to quantify their effect as they get larger. The usefulness of the Kitagawa-Takahashi diagram (Figure 5) is that it can combine the data from these two approaches into a single (stress-based) design criterion. Most stent designs are strain-based, however, because the pulsatile displacements (not stresses) are well characterized in the human body, and Nitinol has a complicated (strain-independent) stress plateau. However, commercial finite-element analysis (FEA) constitutive models, for example, in Ref. 22, can easily resolve these complications, giving the designer a means to determine an accurate stress when only the strains are known.

A more pertinent question may be whether fracture mechanics parameters, such as the stress intensity, can be effectively used to characterize crack growth and to predict lifetimes in materials such as Nitinol that undergo an *in situ* phase transformation. However, in this regard, it is important to note that fracture mechanics descriptions have been widely used to characterize cracking behavior in other phase-transforming materials, such as austenite stainless steels and zirconia ceramics (e.g., Refs. 23 and 24). The most detailed analyses of this problem were performed for the ceramic, partially stabilized zirconia, which undergoes a stress-induced martensitic transformation from a tetragonal to monoclinic phase. Here it was shown that for a fixed global (applied) stress intensity, *in situ* phase transformation did change (i.e., reduced) the local (effective) stress intensity at the crack tip, and that this could be interpreted as a form of toughening.<sup>23,24</sup> Phase transformation can then be considered to toughen the material either by changing the phase into which the crack is propagating (intrinsic toughening) and/or by reducing the effective stress intensity at the crack tip (extrinsic toughening) by crack-tip shielding.<sup>16,25</sup> Although the use of fracture mechanics cannot readily separate these contributions, in the context of this argument, global stress intensities can be utilized as a basis of comparison for the driving force for cracks in different configurations, and the role of the transformation can be construed in terms of changing the materials resistance to fracture.

In similar vein, it is also relevant to consider that such fracture mechanics concepts can become questionable for small cracks in small components where plastic-zone sizes become large compared to component dimensions (where the assumption of small-scale yielding becomes invalid), and/or where crack sizes are small compared to the characteristic dimensions of the microstructure, for example, grain sizes (where assumption of a continuum becomes invalid).<sup>11</sup> This is clearly pertinent to biomedical devices wherein product dimensions can be small (a few hundred micrometers) and typical flaw sizes even smaller (in the tens of micrometers).<sup>10</sup> With respect to the issue of crack

sizes in relation to microstructural size-scales, due to the severe deep drawing necessary to produce superelastic Nitinol tube, grain sizes are in the order of tens of nanometers such that this is not a problem. However, to preserve small-scale yielding conditions, both sample dimensions (e.g., strut width) and flaw sizes must exceed the plastic-zone size by at least an order of magnitude. At near-threshold growth rates, where most of the crack-propagation life is spent,<sup>17</sup> plastic-zone sizes would be in the order of 0.6  $\mu\text{m}$  at  $K \sim 2 \text{ MPa}\sqrt{\text{m}}$ , such that small-scale yielding is appropriate, even for cracks as large as the ASTM F 2063 inclusion size limit of 39  $\mu\text{m}$  for Nitinol. However, for the far less likely failure mode of overload fracture, plastic-zone sizes would exceed  $\sim 16 \mu\text{m}$ , which is only half of the ASTM F 2063 permitted flaw size, such that small-scale yielding would be only strictly valid for  $K < 5 \text{ MPa}\sqrt{\text{m}}$ . Consequently, the fracture-mechanics-based fatigue threshold values that are used in our design diagrams are clearly valid and appropriate even for small biomedical devices; however, the fracture toughness values may become size- and geometry-dependent for small devices where conditions deviate from small-scale yielding.

Finally, as noted earlier, the Kitagawa-Takahashi diagram in Figure 5 was created for simplicity using a geometric factor,  $Y$ , of unity for the stress-intensity solutions. Although reasonable, actual values of this factor will vary depending on the exact device and crack geometries, and this will naturally shift the boundaries between the various regions of behavior. Accordingly, careful finite-element analysis must be performed to accurately calculate that exact stress-intensity solutions in order to create a device-specific Kitagawa-Takahashi design diagram, rather than using the generic one presented herein.

## CONCLUSIONS

In this paper, a simple fracture-mechanics-based approach to design of biomedical devices manufactured from thin-walled ( $\sim 400 \mu\text{m}$  thick) superelastic Nitinol tubing has been presented in terms of device design diagrams which depict safe/unsafe operating regions that are dependent upon the levels of maximum and cyclic stresses experienced by the device from handling, implantation, and *in vivo* operation. To define cumulative fatigue damage mechanisms attributed to cyclic stresses in a device, for example, from pulsatile motion of stent in response to the heartbeat, fatigue-crack growth behavior for both large-crack (experimentally determined) and small-crack (a more conservative interpolation of experimental data) threshold values were evaluated to determine the risk of failure by fatigue. To define failure attributed to single overload events, for example, from deployment stresses in a stent, crack-initiation fracture toughness values were used as the design variable because the small dimensions of most biomedical devices restricts them from ever reaching a higher

steady-state fracture toughness value. A Kitagawa-Takahashi diagram combining traditional “total life” fatigue data with fracture-mechanics-based and yield-stress-based failure criteria was also computed to show safe-operating stresses and stress ranges for devices with known flaw dimensions. Such device design diagrams may be considered as a *conservative* means to define the worst-case susceptibility of a biomedical device to premature failure in the presence of defects, and emphasize the importance of utilizing *both* the traditional (stress-/strain-life) and fracture-mechanics-based approaches to fracture prevention.

Special thanks are due to Drs. Tom Duerig and Alan Pelton of NDC for their financial support and for innumerable helpful discussions on the topic of Nitinol.

## REFERENCES

1. Bonsignore C. A decade of evolution in stent design. In: Pelton AR, Duerig T, editors. Proceedings of the International Conference on Shape Memory and Superelastic Technologies 2003. Menlo Park, CA: SMST Society, Inc.; 2003. pp 519–528.
2. Riepe G, Heintz C, Kaiser E, Chakfé N, Morlock M, Delling M, Imig H. What can we learn from explanted endovascular devices? *Eur J Vasc Endovasc Surg* 2002;24(2):117–122.
3. Jacobs TS, Won J, Gravereaux EC, Faries PL, Morrissey N, Teodorescu VJ, Hollier LH, Marin ML. Mechanical failure of prosthetic human implants: A 10-year experience with aortic stent graft devices. *J Vasc Surg* 2003;37(1):16–26.
4. Allie DE, Hebert CJ, Walker CM. Nitinol stent fractures in the SFA. *Endovasc Today* 2004;7:22–34.
5. Stankiewicz JM, Robertson SW, Ritchie RO. On the fatigue-crack growth properties of thin-walled superelastic austenitic Nitinol tube for endovascular stents. *J Biomed Mater Res A* 22 Dec 2006; epub ahead of print (doi: 10.1002/jbm.a.31100).
6. Robertson SW, Ritchie RO. In vitro fatigue-crack growth and fracture toughness behavior of thin-walled superelastic Nitinol tube for endovascular stents: A basis for defining the effect of crack-like defects. *Biomaterials* 2007;28(4):700–709.
7. American Society of Testing Materials. International Subcommittee E08.06. Standard test method for measurement of fatigue crack growth rates. ASTM Book of Standards, Vol. 3.01, Standard E 647; 2005.
8. American Society of Testing Materials. International Subcommittee E08.06. Standard test method for measurement of the plane strain fracture toughness in metallic materials. ASTM Book of Standards, v. 3.01, Standard E 399; 2005.
9. Pederson OM, Aslaksen A, Vik-Mo H. Ultrasound measurement of the luminal diameter of the abdominal aorta and iliac arteries in patients without vascular disease. *J Vasc Surg* 1993;17(3):596–601.
10. American Society of Testing Materials. International Subcommittee F04.12. Standard specification for wrought nickel-titanium shape memory alloys for medical devices and surgical implants. ASTM Book of Standards, v. 13.01, Standard F 2063; 2006.
11. Ritchie RO, Lankford J. Small fatigue cracks: A statement of the problem and potential solutions. *Mater Sci Eng* 1986;84: 11–16.
12. Hertzberg RW, Herman WA, Ritchie RO. Use of a constant  $K_{\text{max}}$  test procedure to predict small crack growth behavior in 2090-T8E41 aluminum-lithium alloy. *Scripta Metall* 1987;21: 1514–1546.

13. Paris PC, Eredogan F. A critical analysis of crack propagation laws. *J Bas Eng (Trans ASME Ser D)* 1961;85:528–534.
14. Suresh S, Zamiski GF, Ritchie RO. Oxide-induced crack closure: An explanation for near-threshold corrosion fatigue crack growth behavior. *Metall Trans A* 1981;12A:1435–1443.
15. Suresh S, Ritchie RO. A geometric model for fatigue crack closure induced by fracture surface roughness. *Metall Trans A* 1982;13A:1627–1631.
16. Ritchie RO. Mechanisms of fatigue crack propagation in metals, ceramics and composites. *Mater Sci Eng* 1988;103:15–28.
17. Marrey RV, Burgermeister R, Grishaber RB, Ritchie RO. Fatigue and life prediction for cobalt-chromium stents: A fracture mechanics analysis. *Biomaterials* 2006;27:1988–2000.
18. Kitagawa H, Takahashi S. Applicability of fracture mechanics to very small cracks or the cracks in the early stages. In: *Proceedings of the Second International Conference on Mechanical Behavior of Materials*. Metals Park, OH: American Society for Metals; 1976. pp 627–631.
19. Pelton AR, Gong XY, Duerig T. Fatigue testing of diamond specimens. In: Pelton AR, Duerig T, editors. *Proceedings of the International Conference on Shape Memory and Superelastic Technologies*. 2003. pp 293–302.
20. Lopes TL, Gong XY, Trepanier C. Fatigue performance of Nitinol tubing with  $A_f$  of 25°C. In: Pelton AR, Duerig T, editors. *Proceedings of the International Conference on Shape Memory and Superelastic Technologies*. Menlo Park, CA: SMST Society, Inc.; 2003. pp 311–320.
21. Gong XY, Pelton AR, Duerig TW, Rebelo N, Perry K. Finite element analysis and experimental evaluation of superelastic Nitinol stent. In: Pelton AR, Duerig T, editors. *Proceedings of the International Conference on Shape Memory and Superelastic Technologies*. Menlo Park, CA: SMST Society, Inc.; 2003. pp 453–462.
22. Rebelo N, Gong XY, Connally M. Finite element analysis of plastic behavior in Nitinol. In: Pelton AR, Duerig T, editors. *Proceedings of the International Conference on Shape Memory and Superelastic Technologies*. Menlo Park, CA: SMST Society, Inc.; 2003. pp 501–507.
23. Evans AG, Cannon RM. Toughening of brittle solids by martensitic transformation. *Acta Mater* 1986;34:761–800.
24. Evans AG. Perspective on the development of high-toughness ceramics. *J Am Ceram Soc* 1990;73:187–206.
25. Ritchie RO. Mechanisms of fatigue-crack propagation in ductile and brittle solids. *Int J Fracture* 1999;100:55–83.